

Pixel-Wise Feature Selection for Perceptual Edge Detection without post-processing

Hao Shu^{‡*}

[‡] Shenzhen University, Shenzhen, China.

Abstract—Although deep convolutional neural networks (CNNs) have significantly enhanced performance in image edge detection (ED), current models remain highly dependent on post-processing techniques such as non-maximum suppression (NMS), and often fail to deliver satisfactory perceptual results, while the performance will deteriorate significantly if the allowed error toleration distance decreases. These limitations arise from the uniform fusion of features across all pixels, regardless of their specific characteristics, such as the distinction between textural and edge areas. If the features extracted by the ED models are selected more meticulously and encompass greater diversity, the resulting predictions are expected to be more accurate and perceptually meaningful. Motivated by this observation, this paper proposes a novel feature selection paradigm for deep networks that facilitates the differential selection of features and can be seamlessly integrated into existing ED models. By incorporating this additional structure, the performance of conventional ED models is substantially enhanced without post-processing, while simultaneously enhancing the perceptual quality of the predictions. Extensive experimental evaluations validate the effectiveness of the proposed model.

I. INTRODUCTION

Image edge detection (ED) is a fundamental task in computer vision, contributing to a wide range of high-level applications, such as image inpainting[1], object detection[2], and image segmentation[3]. Early works, such as the Sobel operator[4] and Canny algorithm[5], utilized gradients as a criterion to provide efficient edge detectors. Subsequently, statistical methods with hand-crafted features were introduced[6, 7] to enhance performance. In recent years, with the maturation of machine learning research, learning-based algorithms have garnered significant attention[8–13]. Driven by the growing importance of convolutional neural networks (CNNs), numerous CNN-based models have been developed, rapidly establishing themselves as state-of-the-art (SOTA) approaches[14–20].

A satisfactory ED model should exhibit several key properties. Firstly, it must achieve a high precision rate on established benchmarks, providing a numerical demonstration of its capabilities. Secondly, it should generate perceptually accurate results. Finally, it should operate effectively without the need for post-processing techniques, such as non-maximum suppression (NMS). The last term is because as a low-level task, ED is frequently used to support higher-level tasks, where the coefficients of the ED model may need to be optimized jointly with those from other models. NMS,

however, is non-continuous and incompatible with standard optimization procedures.

A fundamental challenge in ED tasks lies in the difficulty of defining edges precisely, which complicates the development of a reliable criterion for distinguishing edge pixels from non-edge pixels. For instance, traditional algorithms like Canny[5] identify edge pixels based on high gradient values, but textural pixels may exhibit similar properties, despite not being edges. This ambiguity in the data necessitates the use of learning-based methods, which can infer the edge pixels from the provided dataset. Consequently, learning-based models, particularly CNN-based approaches[15, 16, 20, 21], have become the mainstream, demonstrating considerable ability and potential in the past decade.

Nevertheless, current research predominantly focuses on feature extraction, with relatively less attention given to feature fusion schemes. For example, many models utilize tens of millions of parameters to extract multi-scale features, but often only fusing them through simple 1×1 convolutional layers. However, the critical issue lies in feature selection. For edge pixels, high-resolution features are more important for accurate detection, while for textural pixels, low-level features should be prioritized, as they often represent background details that should be ignored. In prior ED models, features from all pixels are fused uniformly, typically using a simple 1×1 convolutional layer, which fails to provide effective feature selection. As a result, these models often produce suboptimal outcomes in terms of both accuracy and perceptual quality, particularly in the absence of post-processing. If the features extracted by the ED models are selected more meticulously and encompass greater diversity, the resulting predictions are expected to be more accurate and perceptually meaningful.

Motivated by this observation, this paper introduces a novel feature selection paradigm with a specifically design for ED tasks. This paradigm provides pixel-wise feature selection across varied features, in contrast to previous models, which apply uniform feature fusion across all pixels. To minimize changes to existing models and maximize their utility, the proposed selection model is implemented as an additional block that can be directly integrated into current ED frameworks. This model combines a multi-scale CNN architecture with an encoder-decoder structure in the transformer framework, producing pixel-wise weights employed in feature selection. The final ED model consists of two components: a feature extractor that extracts multi-scale features from a previous ED model, and a pixel-wise feature selector that generates pixel-specific weights to select the most relevant features by a

novel design. Our model significantly outperforms previous ED models that do not incorporate this feature selection structure, as demonstrated by extensive experimental results.

The main contributions of this work are as follows:

- (1) A novel feature selection paradigm is proposed.
- (2) This paradigm is applied to ED tasks, serving as a pixel-wise feature selector that integrates seamlessly into existing feature extraction models to form an enhanced ED framework.
- (3) With the proposed structure, ED models achieve superior numerical and perceptual performance without the need for post-processing.
- (4) Extensive experiments are conducted to validate the effectiveness of the proposed paradigm.

II. PREVIOUS WORK

This section reviews related previous works in the domains of datasets, CNN-based ED models, and the transformer.

A. Datasets

In the early stages of edge detection research, tasks such as edge detection, contour detection, boundary detection, and even segmentation were often treated as similar tasks, utilizing common datasets, most of which were derived from images with segmentation annotations. The most widely used dataset in this domain is the BSDS300, along with its extended version BSDS500[22]. These datasets contain 300 and 500 RGB images, respectively, each annotated by multiple human annotators. They are primarily categorized for contour detection nowadays. Another notable dataset is MDBD[23], which consists of 100 high-resolution (1280×720) images labeled by multiple annotators across 100 different scenes, with 10 sampled frames per scene. It is mainly used for boundary detection tasks currently. The NYUD dataset and its extended version, NYUD2[24], contain hundreds of thousands of indoor scene images, with 1449 labeled images categorized by segmentation. The dataset is primarily used for segmentation tasks, though it has also been employed in edge detection research. Other relevant datasets, including PASCAL VOC[25], Microsoft COCO[26], SceneParse150[27], and Cityscape[28], have also been utilized in early edge detection studies.

Although these datasets can be used for edge detection, the increasing specificity of the research has led to the development of dedicated ED datasets. One such dataset is BIPED[29], later modified to BIPED2, introduced in 2020. It consists of 250 high-resolution (1280×720) RGB images with edge annotations. Another dataset, BRIND[30], was proposed in 2021, which re-annotates the BSDS500 dataset, classifying edges into four categories: reflectance edges, illumination edges, normal edges, and depth edges. The UDED dataset[31], proposed in 2023, contains 29 high-quality images selected from previous datasets with careful annotations. Despitensess, the small size of the dataset limits its broader application.

Human annotations remain essential for ED tasks, as they could be the only way to provide the groundtruth. However, human labeling is inherently subjective and prone to noise. Missing or erroneous labels can be significant, and annotations may vary even from the same person twice. To address these

issues, recent studies have focused on improving label quality and enhancing model performance in the presence of noisy labels[32–34].

B. Models

Edge detection is one of the most foundational tasks in image processing, with a history predating the widespread use of computers. Early methods such as the Canny[5] and Sobel[4] operators focused on gradient-based features, which are simple yet effective for detecting edges. These methods remain widely applied in computer vision tasks due to their simplicity and efficiency. Later works introduced statistical methods and pioneering learning-based models that integrated various hand-crafted features, such as Chernoff information[6], histograms[7], brightness, color, textures[8], and sketch tokens[11]. These models employed various techniques, such as structured forests[11, 13], nearest-neighbor search[12], and logistic regression[10], to train classifiers. Despite the improvements made by these methods, they faced a bottleneck in accurately distinguishing edge cues from textural features.

With the rise of deep learning, deep models for edge detection gained prominence in the past decade, demonstrating substantial improvements in performance. The Holistically-Nested Edge Detection (HED) model[15] utilizes multi-scale features across multiple layers to extract edge cues. Such a framework has become the mainstream approach for edge detection. The Richer Convolutional Features (RCF) model[16] further refines feature extraction by utilizing features from different layers at various levels. The Bi-Directional Cascade Network (BDCN)[21] incorporates multiple supervision signals across different scales to enhance edge detection accuracy, while the Pixel Difference Network (PiDiNet)[19] introduces pixel difference convolutions to improve CNN efficiency. RIND[30] fuses four types of edges at three stages, and Dexi[20] employs highly dense skip connections to improve edge prediction.

Most of these models are supervised using weighted binary cross-entropy (WBCE) loss, which ensures high precision but often fails to produce crisp edges without post-processing techniques like non-maximum suppression (NMS). To address this issue, some studies have explored alternative loss functions, such as Dice loss[35] and tracing loss[36], which aim to generate thinner edges. While these loss functions can yield more perceptual results, they may sacrifice some precision.

C. Encoder-Decoder Framework in Transformers

The encoder-decoder framework, initially developed for natural language processing[37], has proven effective in image processing tasks as well[38]. Models based on this framework are able to capture long-range dependencies without requiring very deep architectures, in contrast to convolutional neural networks (CNNs). The effectiveness of transformer-based models has been demonstrated in various image tasks, including object detection[39], semantic segmentation[40], and super-resolution[41]. Recently, transformer-based models have also been applied to edge detection tasks[42], further expanding their utility in image processing.

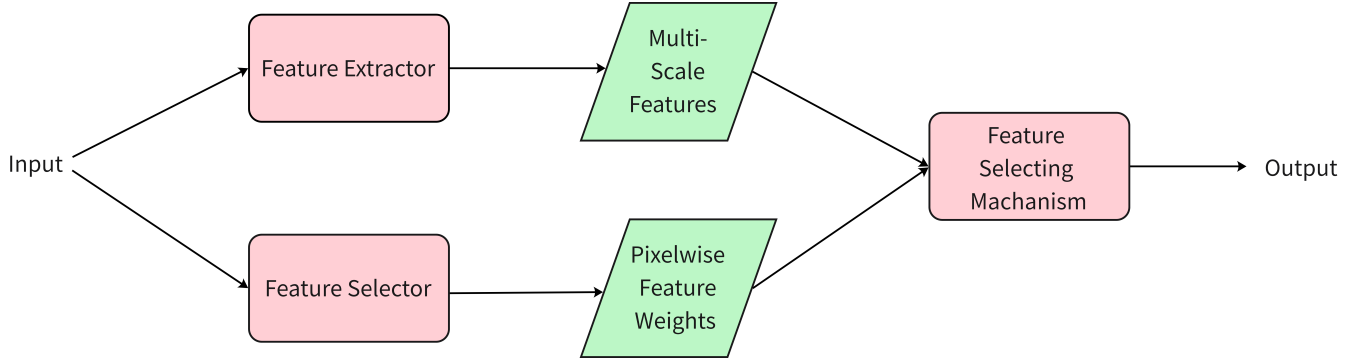


Fig. 1 The framework of the selecting paradigm consists of two parts, a feature extractor and a feature selector. The extractor directly employs a previous model, while the selector is newly designed. The multi-scale features outputted by the extractor are selected by the selector which provides pixel-wise weights. The final feature selecting mechanism multiplies the weights and the features and then sums over channels to obtain the weighted average.

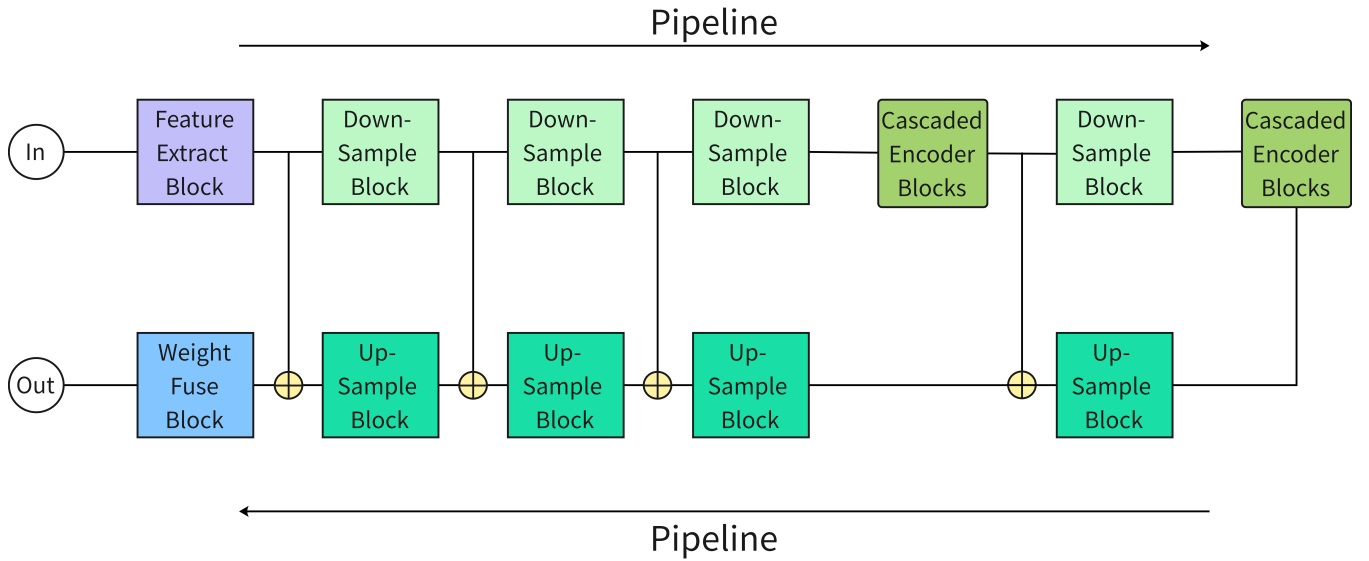


Fig. 2 The feature selector is designed as a downscale-upscale structure with residual connections. The input images are first gone through a feature extract block, and then $\frac{1}{2}$ -down-sample four times to obtain multi-scale features. Moreover, in $\frac{1}{8}$ and $\frac{1}{16}$ scales, cascaded encoder blocks, typically 6, from transformer are applied. The $\frac{1}{16}$ -scale features are up-sampled step by step with twice each to rescale the features to the ordinary scale. Each up-sample block is followed by a residual connection with a learnable weight balancing the up-sample features and the features provided by the residual connection. Finally, the ordinary-scale features are fused to output pixel-wise weights which will be later employed in selecting mechanism. Details of each block will be displayed in the following figures.

III. METHODOLOGY

A. Overview of the architecture

The proposed feature selection architecture consists of two primary components: a feature extractor that captures multi-scale features from the input images, and a feature selector that assigns pixel-wise weights to these features. The feature extractor leverages established models such as HED[15], RCF[16], BDCN[21], and Dexi[20]. The feature selector, on the other hand, is designed using a hybrid structure that combines CNN and the encoder-decoder framework in transformers, as detailed in the following subsection. An abstract overview of the framework is shown in Figure1.

B. Design of the selection model

The feature selector is designed by integrating CNN with the encoder-decoder framework in transformer. The utility of CNN

in image processing is well-established, while the effectiveness of transformers has gained considerable attention in recent studies. CNN excels at capturing short-range features, whereas the attention mechanism in transformers is adept at modeling long-range dependencies with a relatively shallow architecture. Thus, combining these two structures is expected to result in a model that can efficiently process both short-range and long-range features.

The architecture of the feature selector is illustrated in Figure2. The model follows a U-Net-like framework commonly employed in CNN-based ED models. However, at the $\frac{1}{8}$ and $\frac{1}{16}$ scales, the encoder-decoder structure is integrated. The final fusion stage employs a three-layer structure as used in SDPED[34], which has demonstrated superior performance in ED tasks through extensive experiments. Additionally, trainable coefficients are introduced within the residual connections

to optimize the balance between the output features and the features linked through the residuals.

The details of the blocks are displayed in Figure3, Figure4, Figure5, Figure6, Figure7, Figure8.

C. Training method

The model is trained in three distinct stages. In stage 1, the feature extractor is trained using its default loss function. In stage 2, the coefficients of the extractor are frozen, and the feature selector is trained using the L_{WBCE} loss function. In the final stage 3, both the feature extractor and selector are trained simultaneously using the L_{WBCE} loss function. The weight binary cross-entropy (WBCE) loss is defined as:

$$L_{WBCE}(\hat{Y}, Y) = -\alpha \sum_{\hat{y}_i \in Y^+} \log(\hat{y}_i) - \lambda(1-\alpha) \sum_{y_i \in Y^-} \log(1-\hat{y}_i) \quad (1)$$

where Y^+ represents the set of edge pixels in the ground truth (positive samples), Y^- denotes the set of non-edge pixels (negative samples), and $\alpha = \frac{|Y^-|}{|Y|}$, with $\lambda = 1.1$. This loss function ensures that the model is optimized to predict accurate edge detection results by emphasizing both precision and recall.

IV. EXPERIMENT

A. Settings and benchmarks

The experimental setup and evaluation benchmarks follow the approach outlined in[34], with the details provided below.

1) *Dataset and Data augmentation*: The models are evaluated on three datasets: BRIND[30], UDED[31], and BIPED[29]. For the BRIND dataset, all edge labels are combined to create a binary groundtruth map for each image. In contrast, the UDED and BIPED datasets contain unique annotations for edge detection, which are directly employed. Here, the dataset BRIND consisting with 500 images is randomly split into 400 training ones and 100 evaluation ones, the dataset BIPED2 consisting of 250 images is randomly split into 200 training ones and 50 evaluation ones, following the standard 2:8 benchmark, while the 27 images in dataset UDED are randomly split into 20 training ones and 7 evaluation ones.

During training, all images are split halved such that their height and width are both reduced to below 640 pixels. Subsequently, images are augmented with rotations (0° , 90° , 180° , and 270°) and horizontal flips. To enhance the model performance, noiseless data are added to the training set as in[34]. Images are then randomly cropped to 320×320 pixels and refreshed every 5 epochs during training. Additionally, images from UDED with width or height smaller than 320 pixels are aborted.

2) *Optimizer and training epochs*: All models are trained using the Adam optimizer with a weight decay of 10^{-8} . The learning rate is set to 10^{-4} . The batch size is set to 8.

The training process is organized into three distinct stages. In the first stage, the feature extractor is trained independently, with training durations of 50 epochs for the BRIND and BIPED2 datasets, and 200 epochs for the UDED dataset. The

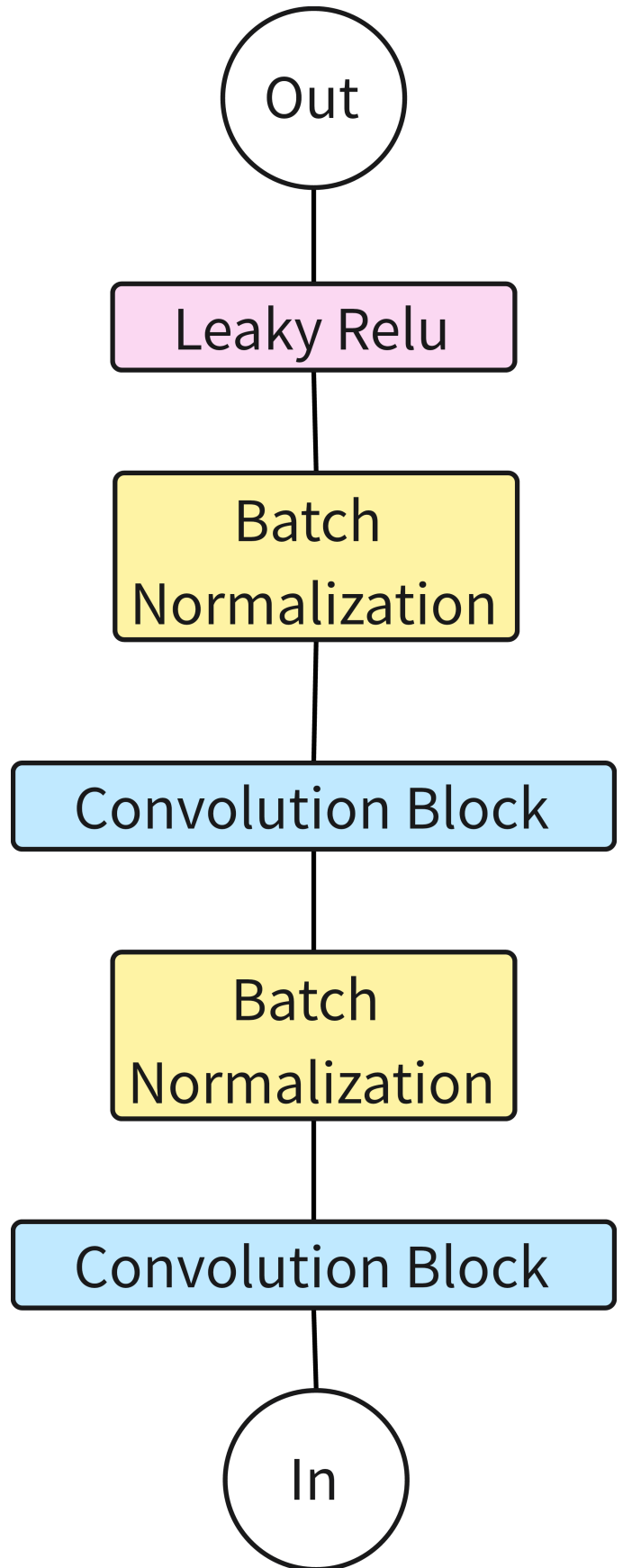


Fig. 3 The feature extract block consists of standard 2 convolution layers, each followed by a batch normalization layer, and finally a activating function employing Leaky Relu. The convolution layers here are all 3×3 .

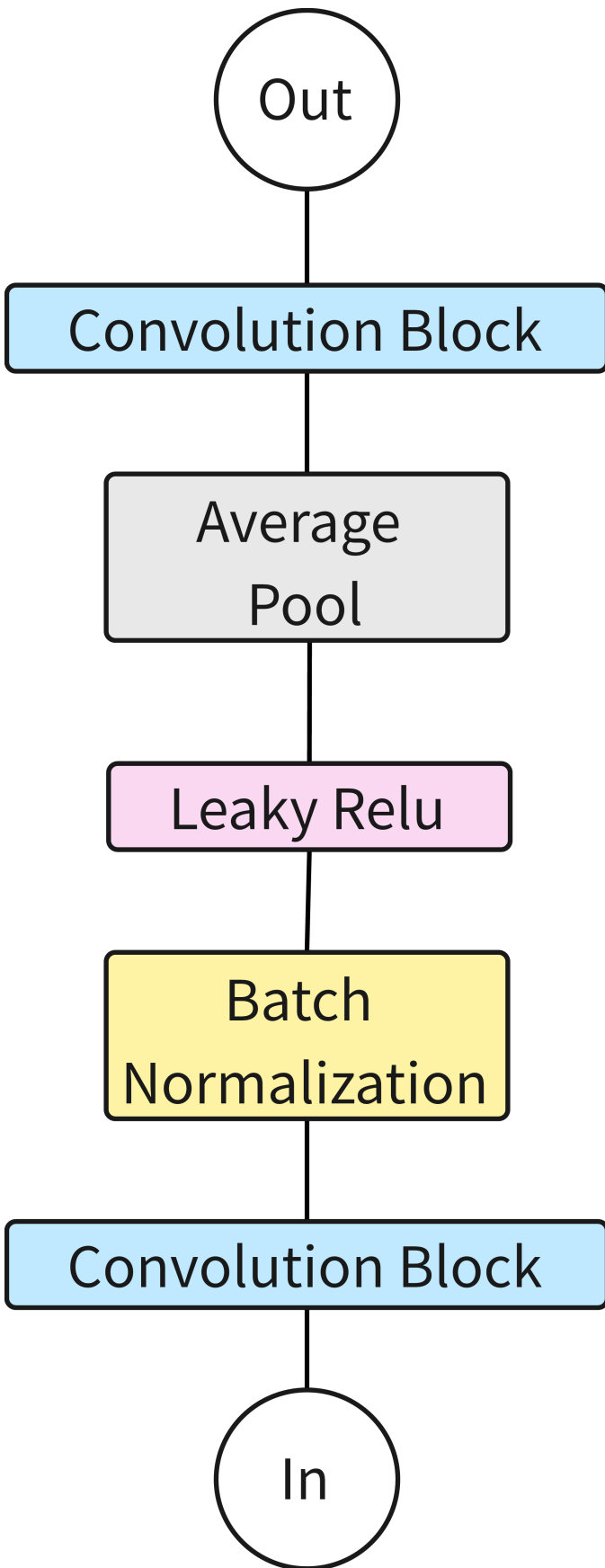


Fig. 4 The down-sample block employs the 3×3 average-pool operation with stride 2. The input features firstly go through a 3×3 convolution layer, followed by batch normalization and activating function Leaky Relu. Then the average-pool is applied. Finally, another convolution layer is accessed.

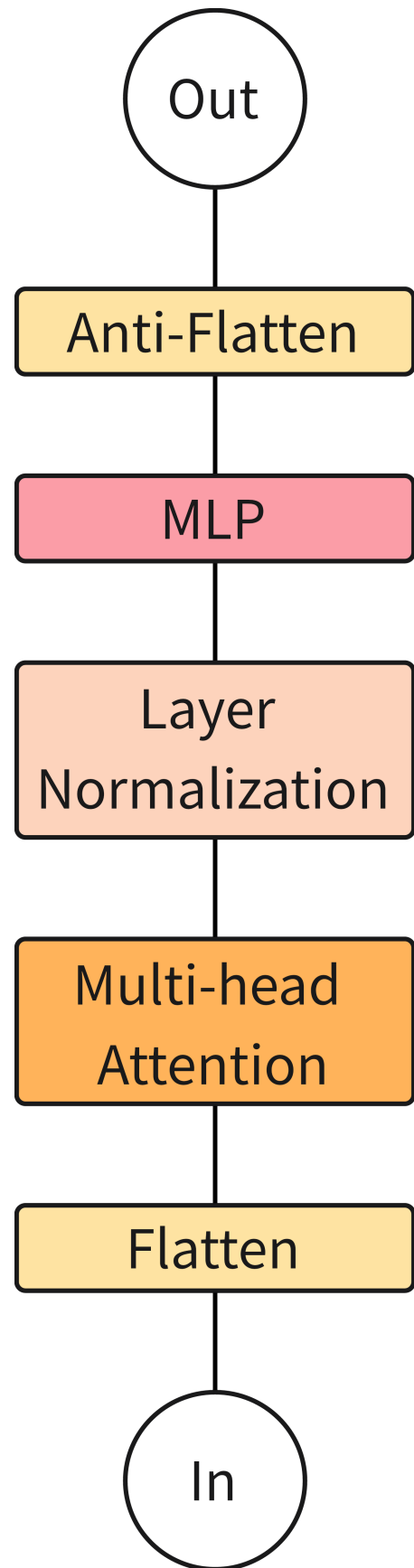


Fig. 5 The encoder block of the transformer in image tasks typically includes a flatten operation, a multi-head attention layer, a layer-normalization operation, and a MLP. Here, the flatten operation flattens the 2D images into 1D vectors that can be accessed in the multi-head attention layer. The multi-head attention layer typically employs 8 heads and output the attention results. The MLP further processes the features and the features are finally folded back to 2D images.

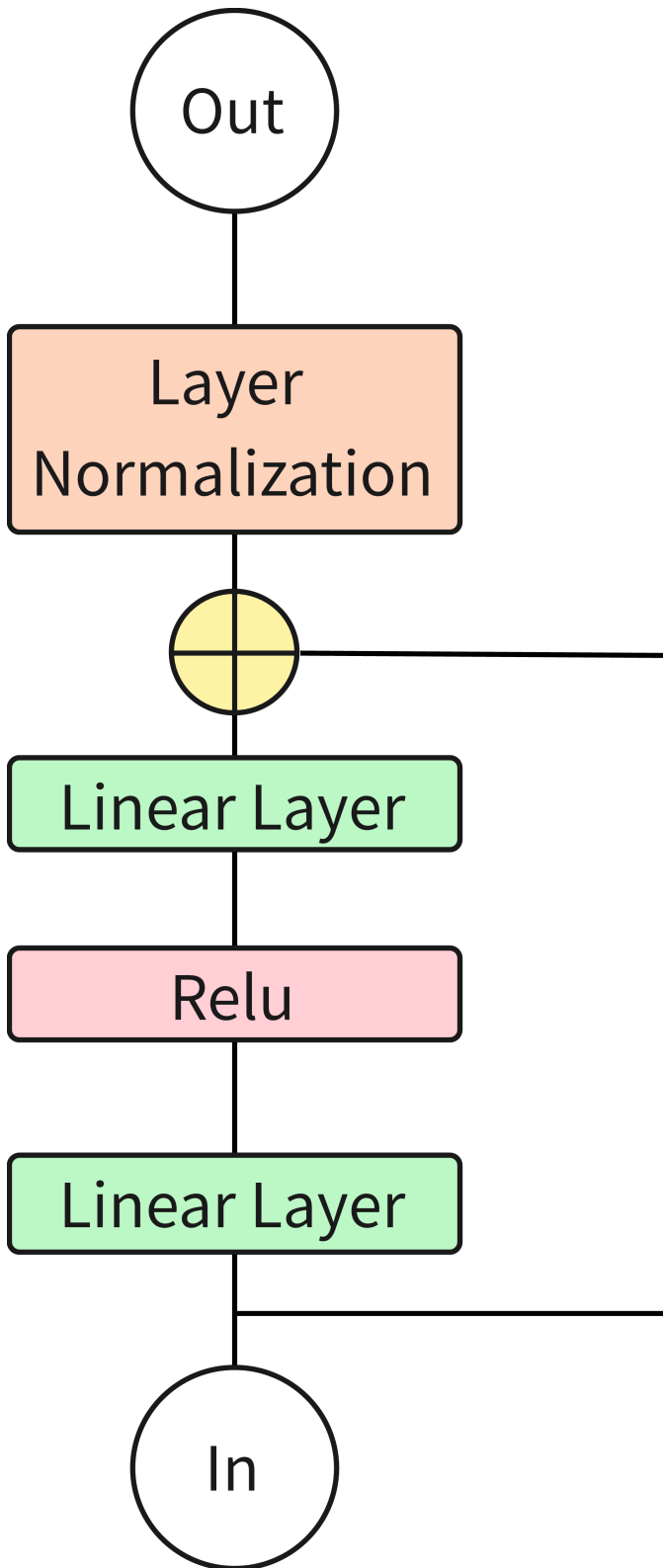


Fig. 6 The MLP is typical. It includes two linear layers with activating function Relu, residual connection, and layer normalization.

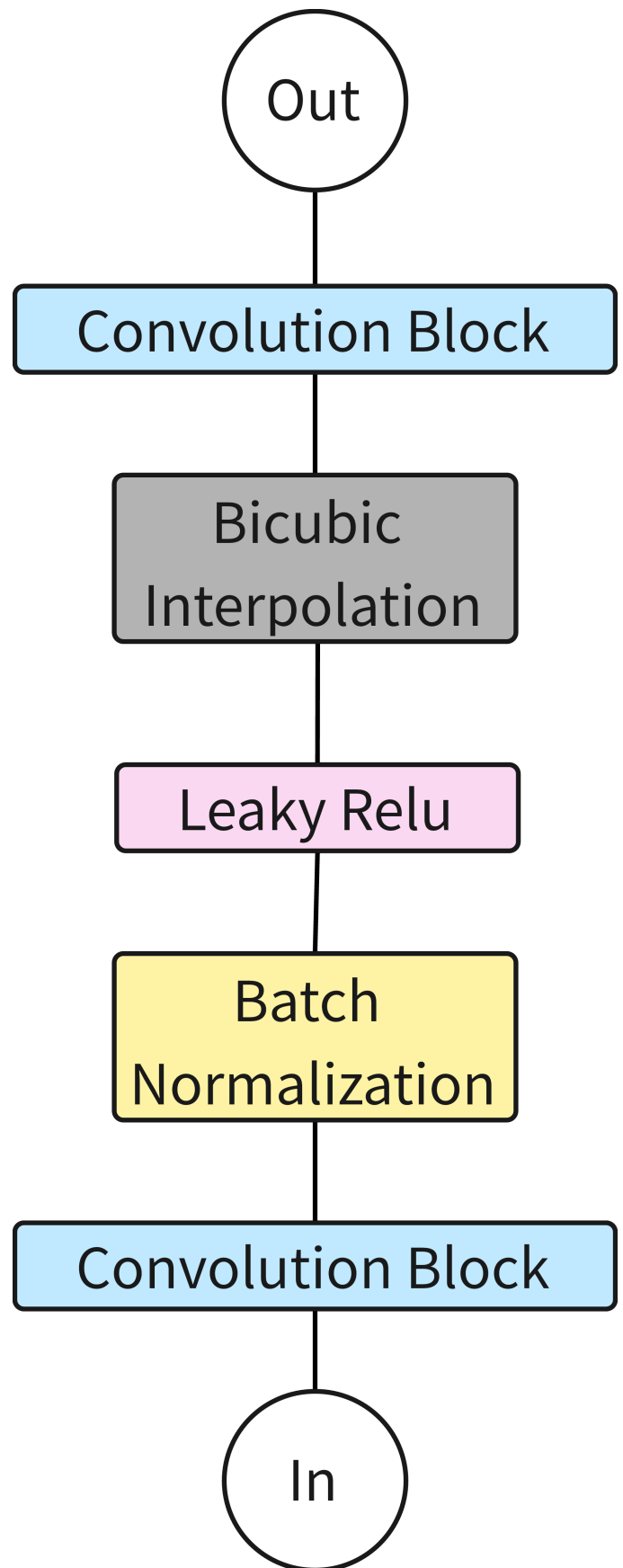


Fig. 7 The up-sample replaces the average-pool operation with the $\times 2$ bi-cubic interpolation operation. Other structures are similar to the down-sample block. The convolution layers here are all 3×3 .

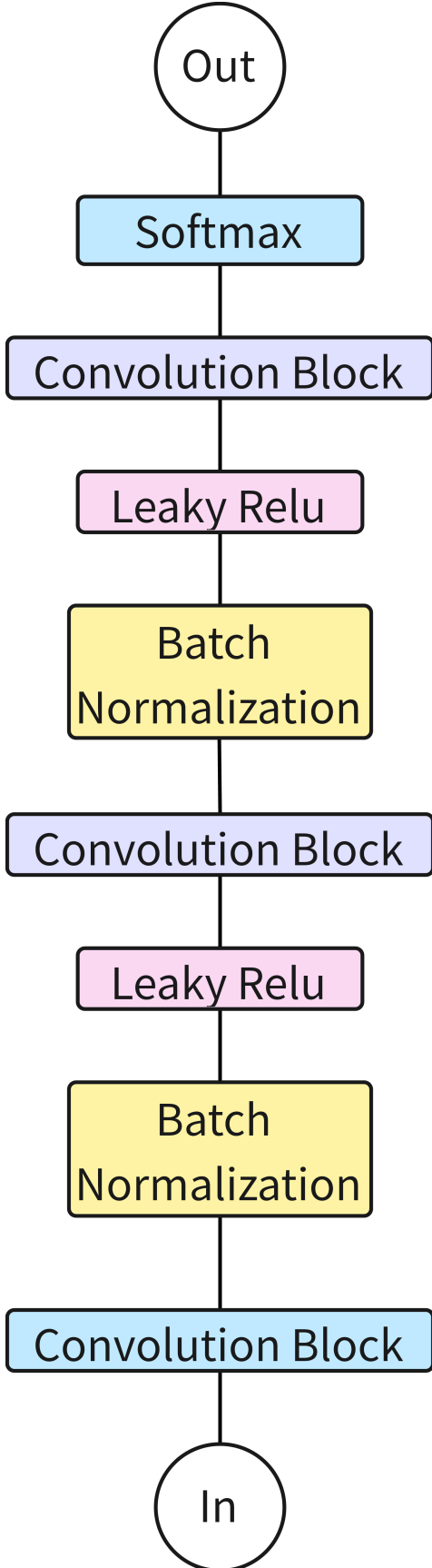


Fig. 8 The final weight fuse block consists of the following operations. Firstly, the features go through a 3×3 convolution layer followed by a batch normalization and an activating function Leaky Relu. Then they are processed by the same structure but the convolution layer is replaced by a 1×1 one. Finally, another 1×1 convolution layer is accessed and the Softmax function is applied to provide the pixel-wise weights.

second stage focuses on training the feature selector while keeping the feature extractor fixed, with training taking an additional 50 epochs for BRIND and BIPED2, and 200 epochs for UDED. In the final stage, both the feature extractor and the feature selector are trained jointly, with this stage lasting another 50 epochs for BRIND and BIPED2, and 200 epochs for UDED.

3) *Evaluation benchmarks*: Model performance is evaluated using the methodology described in[8], calculating the Optimal Dataset Scale (ODS), Optimal Image Scale (OIS), and Average Precision (AP) under an error tolerance distances. To maintain a high standard, the error tolerance is set to 1 pixel, as discussed in[34].

To assess the effectiveness of the proposed feature selector, we compare models with and without the selector, as well as with or without the union training stage 3, using the HED[15], RCF[16], BDCN[21], and Dexi[20] as extractors. All models are trained (or retrained) under the same settings to ensure a fair comparison. A prediction is obtained piece by piece with 320×320 sub-images and then integrated together.

B. Experiment results

TABLE I

Results on BIPED2 with 1 pixel error tolerance, without NMS. For each extractor, the first row presents results for the standard feature extractor, the second row (-S) indicates results for the extractor combined with the selector without union training, and the third row (-S-U) represents results with additional union training. The best score among the three configurations is highlighted in bold. Improvements relative to the standard extractor are indicated in parentheses. The last two rows report average improvements (AI) across the four models, including with and without union training.

	BIPED2 without NMS		
	ODS	OIS	AP
HED	0.592	0.602	0.347
HED-S	0.649 (+9.63%)	0.654 (+8.64%)	0.433 (+24.78%)
HED-S-U	0.655 (+10.64%)	0.663 (+10.13%)	0.491 (+41.50%)
RCF	0.591	0.597	0.345
RCF-S	0.641 (+8.46%)	0.645 (+8.04%)	0.418 (+21.16%)
RCF-S-U	0.666 (+12.69%)	0.672 (+12.56%)	0.502 (+45.51%)
BDCN	0.629	0.635	0.421
BDCN-S	0.633 (+0.64%)	0.639 (+0.63%)	0.423 (+0.46%)
BDCN-S-U	0.661 (+5.09%)	0.666 (+4.88%)	0.484 (+14.96%)
Dexi	0.632	0.636	0.432
Dexi-S	0.640 (+1.27%)	0.644 (+1.26%)	0.441 (+2.08%)
Dexi-S-U	0.650 (+2.89%)	0.656 (+3.14%)	0.465 (+7.64%)
AI-S	+5.00%	+4.64%	+12.12%
AI-S-U	+7.83%	+7.68%	+27.40%

The evaluation results on the BIPED2, UDED, and BRIND datasets, without post-processing, are presented in Table I, Table II, and Table III, respectively. Some representative predicted images are shown in Fig ???. With the proposed feature selection paradigm, the models achieve significantly improved performance across all datasets and nearly all benchmarks.

On average, across the four models, the feature selection paradigm leads to improvements of 5.00% / 7.83%, 4.64% / 7.68%, and 12.12% / 27.40% on the BIPED2 dataset, 2.24% / 2.16%, 1.93% / 1.63%, and 9.46% / 19.23% on the BRIND dataset, and 2.33% / 5.28%, 2.01% / 3.62%, and 9.62% / 21.74% on the UDED dataset, measured by ODS, OIS, and AP, respectively, both with and without union training.

TABLE II

Results on BRIND with 1 pixel error tolerance, without NMS. The table structure and explanations are identical to those in Table I, with results for the BRIND dataset.

	BRIND without NMS		
	ODS	OIS	AP
HED	0.645	0.656	0.417
HED-S	0.668 (+3.57%)	0.677 (+3.20%)	0.466 (+11.75%)
HED-S-U	0.668 (+3.57%)	0.673 (+2.59%)	0.522 (+25.18%)
RCF	0.646	0.656	0.394
RCF-S	0.667 (+3.25%)	0.675 (+2.90%)	0.475 (+20.56%)
RCF-S-U	0.666 (+3.10%)	0.672 (+2.44%)	0.517 (+31.22%)
BDCN	0.659	0.672	0.467
BDCN-S	0.668 (+1.37%)	0.677 (+0.74%)	0.486 (+4.07%)
BDCN-S-U	0.672 (+1.97%)	0.681 (+1.34%)	0.516 (+10.49%)
Dexi	0.666	0.672	0.478
Dexi-S	0.671 (+0.75%)	0.678 (+0.89%)	0.485 (+1.46%)
Dexi-S-U	0.666 (+0.00%)	0.673 (+0.15%)	0.529 (+10.04%)
AI-S	+2.24%	+1.93%	+9.46%
AI-S-U	+2.16%	+1.63%	+19.23%

TABLE III

Results on UDED with 1 pixel error tolerance at the lowest resolution, without NMS. The table structure and explanations are identical to those in Table I, with results for the UDED dataset.

	UDED without NMS		
	ODS	OIS	AP
HED	0.716	0.751	0.489
HED-S	0.733 (+2.37%)	0.764 (+1.73%)	0.521 (+6.54%)
HED-S-U	0.723 (+0.98%)	0.751 (+0.00%)	0.602 (+23.11%)
RCF	0.699	0.741	0.450
RCF-S	0.723 (+3.43%)	0.761 (+2.70%)	0.562 (+24.89%)
RCF-S-U	0.752 (+7.58%)	0.781 (+5.40%)	0.635 (+41.11%)
BDCN	0.706	0.744	0.530
BDCN-S	0.727 (+2.97%)	0.764 (+2.69%)	0.569 (+7.36%)
BDCN-S-U	0.758 (+7.37%)	0.778 (+4.57%)	0.625 (+17.92%)
Dexi	0.733	0.752	0.600
Dexi-S	0.737 (+0.55%)	0.759 (+0.93%)	0.598 (-0.33%)
Dexi-S-U	0.771 (+5.18%)	0.786 (+4.52%)	0.629 (+4.83%)
AI-S	+2.33%	+2.01%	+9.62%
AI-S-U	+5.28%	+3.62%	+21.74%

V. CONCLUSION

In this paper, we introduced a novel paradigm for image-related tasks, referred to as the selecting paradigm, which was applied to develop a feature selector for edge detection (ED) models. Our extensive experiments demonstrate that models equipped with this selector achieve significant improvements in both perceptual quality and evaluation scores across three datasets. Moreover, the selecting paradigm is compatible with existing models, allowing seamless integration without requiring major architectural changes, thereby enhancing the convenience of its deployment. This adaptability positions the paradigm as a powerful and practical tool for improving model performance.

VI. BIBLIOGRAPHY

REFERENCES

- [1] K. Nazeri, E. Ng, T. Joseph, F. Qureshi, and M. Ebrahimi. Edgeconnect: Structure guided image inpainting using edge prediction. In *2019 IEEE/CVF International Conference on Computer Vision Workshop (ICCVW)*, pages 3265–3274, 2019.
- [2] C. H. Zhan, X. H. Duan, S. Y. Xu, Z. Song, and M. Luo. An improved moving object detection algorithm based on frame difference and edge detection. In *Fourth international conference on image and graphics (ICIG 2007)*, pages 519–523. IEEE, 2007.
- [3] R. Muthukrishnan and M. Radha. Edge detection techniques for image segmentation. *International Journal of Computer Science & Information Technology*, 3(6):259, 2011.
- [4] J. Kittler. On the accuracy of the sobel edge detector. *Image and Vision Computing*, 1(1):37–42, 1983.
- [5] J. Canny. A computational approach to edge detection. *IEEE Transactions on pattern analysis and machine intelligence*, PAMI-8(6):679–698, 1986.
- [6] S. Konishi, A. L. Yuille, J. M. Coughlan, and S. C. Zhu. Statistical edge detection: learning and evaluating edge cues. *IEEE Transactions on Pattern Analysis and Machine Intelligence*, 25(1):57–74, 2003.
- [7] P. Arbeláez, M. Maire, C. Fowlkes, and J. Malik. Contour detection and hierarchical image segmentation. *IEEE Transactions on Pattern Analysis and Machine Intelligence*, 33(5):898–916, 2011.
- [8] D.R. Martin, C.C. Fowlkes, and J. Malik. Learning to detect natural image boundaries using local brightness, color, and texture cues. *IEEE Transactions on Pattern Analysis and Machine Intelligence*, 26(5):530–549, 2004.
- [9] P. Dollar, Z. W. Tu, and S. Belongie. Supervised learning of edges and object boundaries. In *2006 IEEE Computer Society Conference on Computer Vision and Pattern Recognition (CVPR'06)*, volume 2, pages 1964–1971, 2006.
- [10] X. F. Ren. Multi-scale improves boundary detection in natural images. In *Computer Vision–ECCV 2008: 10th European Conference on Computer Vision, Marseille, France, October 12–18, 2008, Proceedings, Part III 10*, pages 533–545. Springer, 2008.

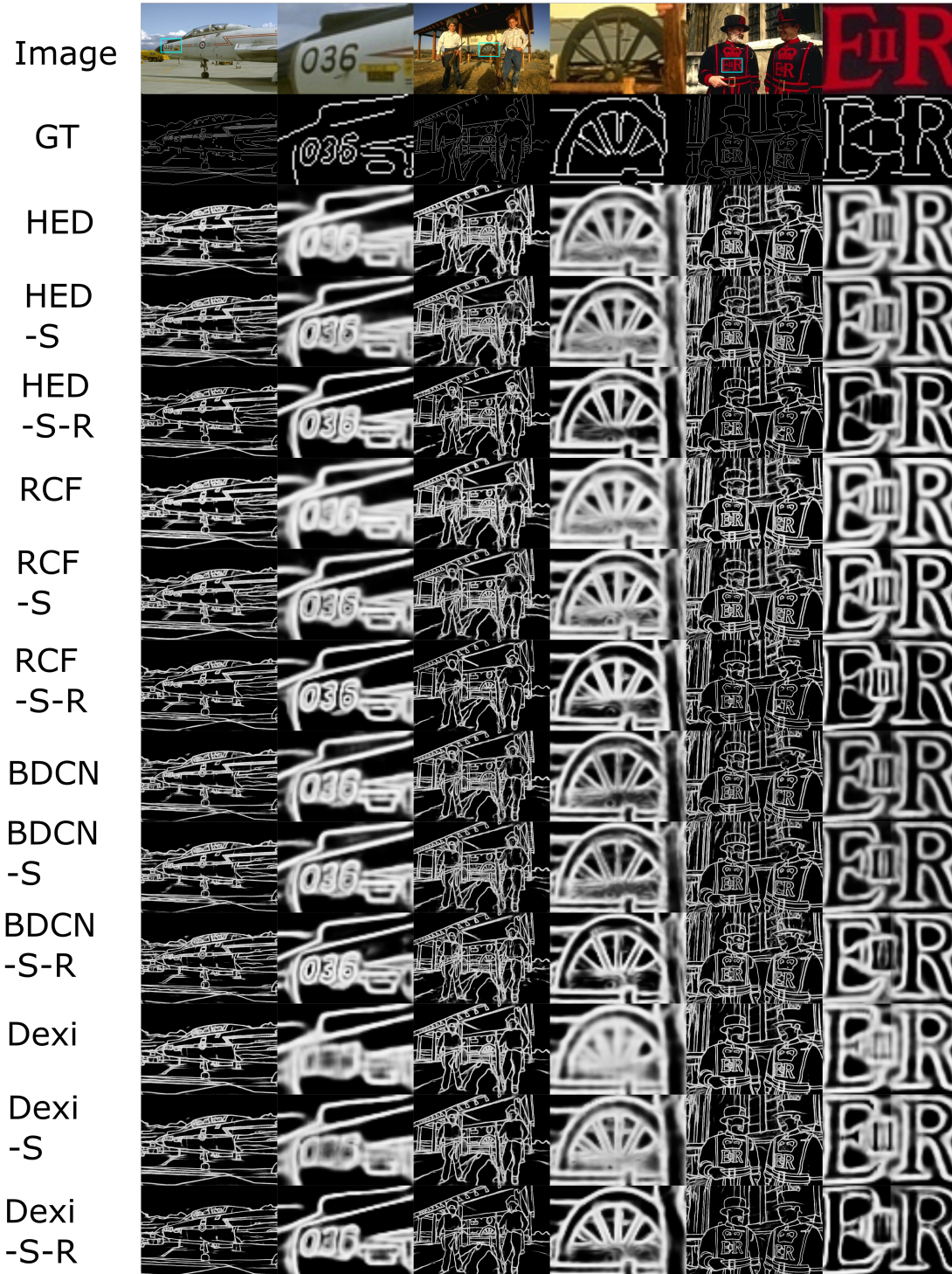


Fig. 9 The 1, 3, 5 columns are the full images and the 2, 4, 6 columns are the cut images from the blue boxes. The rows represent the ordinary images(Image), the groundtruthes(GT), and the predictions of the models, respectively. -S indicates results for the extractor combined with the selector without union training, and -S-U represents results with additional union training.

- [11] J. J. Lim, C. L. Zitnick, and P. Dollár. Sketch tokens: A learned mid-level representation for contour and object detection. In *Proceedings of the IEEE conference on computer vision and pattern recognition*, pages 3158–3165, 2013.
- [12] Y. Ganin and V. Lempitsky. n^4 -fields: neural network nearest neighbor fields for image transforms. In *Asian conference on computer vision*, pages 536–551. Springer, 2014.
- [13] P. Dollár and C. L. Zitnick. Fast edge detection using structured forests. *IEEE Transactions on Pattern Analysis and Machine Intelligence*, 37(8):1558–1570, 2015.
- [14] G. Bertasius, J. B. Shi, and L. Torresani. Deepedge: A multi-scale bifurcated deep network for top-down contour detection. In *Proceedings of the IEEE conference on computer vision and pattern recognition*, pages 4380–4389, 2015.
- [15] S. N. Xie and Z. W. Tu. Holistically-nested edge detection. In *Proceedings of the IEEE international conference on computer vision*, pages 1395–1403, 2015.
- [16] Y. Liu, M. M. Cheng, X. W. Hu, K. Wang, and X. Bai. Richer convolutional features for edge detection. In *Proceedings of the IEEE conference on computer vision and pattern recognition*, pages 3000–3009, 2017.
- [17] J. Z. He, S. L. Zhang, M. Yang, Y. H. Shan, and T. J. Huang. Bi-directional cascade network for perceptual edge detection. In *Proceedings of the IEEE/CVF conference on computer vision and pattern recognition*, pages 3828–3837, 2019.
- [18] M. Le and S. Kayal. Revisiting edge detection in convolutional neural networks. In *2021 International Joint Conference on Neural Networks (IJCNN)*, pages 1–9. IEEE, 2021.
- [19] Z. Su, W. Z. Liu, Z. T. Yu, D. W. Hu, Q. Liao, Q. Tian, M. Pietikäinen, and L. Liu. Pixel difference networks for efficient edge detection. In *Proceedings of the IEEE/CVF international conference on computer vision*, pages 5117–5127, 2021.
- [20] X. Soria, A. Sappa, P. Humanante, and A. Akbarinia. Dense extreme inception network for edge detection. *Pattern Recognition*, 139:109461, 2023.
- [21] J. Z. He, S. L. Zhang, M. Yang, Y. H. Shan, and T. J. Huang. Bdcn: Bi-directional cascade network for perceptual edge detection. *IEEE Transactions on Pattern Analysis and Machine Intelligence*, 44(1):100–113, 2022.
- [22] D. Martin, C. Fowlkes, D. Tal, and J. Malik. A database of human segmented natural images and its application to evaluating segmentation algorithms and measuring ecological statistics. In *Proc. 8th Int'l Conf. Computer Vision*, volume 2, pages 416–423, July 2001.
- [23] D. A. Mély, J. k. Kim, M. McGill, Y. L. Guo, and T. Serre. A systematic comparison between visual cues for boundary detection. *Vision Research*, 120:93–107, 2016. Vision and the Statistics of the Natural Environment.
- [24] N. N. Silberman, D. Hoiem, P. P. Kohli, and R. Fergus. Indoor segmentation and support inference from rgb-d images. In *European Conference on Computer Vision*, 2012.
- [25] M. Everingham, L. Van Gool, C. K. I. Williams, J. Winn, and A. Zisserman. The pascal visual object classes (voc) challenge. *International Journal of Computer Vision*, 88(2):303–338, jun 2010.
- [26] T. Y. Lin, M. Maire, S. Belongie, L. Bourdev, R. Girshick, J. Hays, P. Perona, D. Ramanan, C. L. Zitnick, and P. Dollár. Microsoft coco: Common objects in context. In *Computer Vision – ECCV 2014*, pages 740–755. Springer International Publishing, 2014.
- [27] B. L. Zhou, H. Zhao, X. Puig, S. Fidler, A. Barriuso, and A. Torralba. Scene parsing through ade20k dataset. In *2017 IEEE Conference on Computer Vision and Pattern Recognition (CVPR)*, pages 5122–5130, 2017.
- [28] M. Cordts, M. Omran, S. Ramos, T. Rehfeld, M. Enzweiler, R. Benenson, U. Franke, S. Roth, and B. Schiele. The cityscapes dataset for semantic urban scene understanding. In *Proceedings of the IEEE Conference on Computer Vision and Pattern Recognition (CVPR)*, June 2016.
- [29] X. Soria, E. Riba, and A. Sappa. Dense extreme inception network: Towards a robust cnn model for edge detection. In *2020 IEEE Winter Conference on Applications of Computer Vision (WACV)*, pages 1912–1921. IEEE Computer Society, mar 2020.
- [30] M. Pu, Y. Huang, Q. Guan, and H. Ling. Rindnet: Edge detection for discontinuity in reflectance, illumination, normal and depth. In *2021 IEEE/CVF International Conference on Computer Vision (ICCV)*, pages 6859–6868. IEEE Computer Society, oct 2021.
- [31] X. Soria, Y. Li, M. Rouhani, and A. D. Sappa. Tiny and efficient model for the edge detection generalization. In *2023 IEEE/CVF International Conference on Computer Vision Workshops (ICCVW)*, pages 1356–1365. IEEE Computer Society, oct 2023.
- [32] Y. B. Fu and X. J. Guo. Practical edge detection via robust collaborative learning. In *Proceedings of the 31st ACM International Conference on Multimedia, MM '23*, page 2526–2534. Association for Computing Machinery, 2023.
- [33] C. Wang, D. Dai, S. Xia, Y. Liu, and G. Wang. One-stage deep edge detection based on dense-scale feature fusion and pixel-level imbalance learning. *IEEE Transactions on Artificial Intelligence*, 5(01):70–79, jan 2024.
- [34] Hao Shu. More precise edge detections. 2024.
- [35] R. X. Deng, C. H. Shen, S. J. Liu, H. B. Wang, and X. R. Liu. Learning to predict crisp boundaries. In *Computer Vision – ECCV 2018: 15th European Conference, Munich, Germany, September 8–14, 2018, Proceedings, Part VI*, page 570–586. Springer-Verlag, 2018.
- [36] L. X. Huan, N. Xue, X. W. Zheng, W. He, J. Y. Gong, and G. S. Xia. Unmixing convolutional features for crisp edge detection. *IEEE Trans. Pattern Anal. Mach. Intell.*, 44(10 Part 1):6602–6609, oct 2022.
- [37] A. Vaswani, N. Shazeer, N. Parmar, J. Uszkoreit, L. Jones, A. N. Gomez, L. Kaiser, and I. Polosukhin. Attention is all you need. In *Advances in Neural Information Processing Systems*, volume 30. Curran Associates,

- Inc., 2017.
- [38] A. Dosovitskiy. An image is worth 16x16 words: Transformers for image recognition at scale. *arXiv preprint arXiv:2010.11929*, 2020.
 - [39] N. Carion, F. Massa, G. Synnaeve, N. Usunier, A. Kirillov, and S. Zagoruyko. End-to-end object detection with transformers. In *European conference on computer vision*, pages 213–229. Springer, 2020.
 - [40] S. X. Zheng, J. C. Lu, H. S. Zhao, X. T. Zhu, Z. K. Luo, Y. B. Wang, Y. W. Fu, J. F. Feng, T. Xiang, P. H. S. Torr, and L. Zhang. Rethinking semantic segmentation from a sequence-to-sequence perspective with transformers. In *Proceedings of the IEEE/CVF conference on computer vision and pattern recognition*, pages 6881–6890, 2021.
 - [41] X. Zhang, Y. L. Zhang, and F. Yu. Hit-sr: Hierarchical transformer for efficient image super-resolution. In *European Conference on Computer Vision*, pages 483–500. Springer, 2025.
 - [42] M. Y. Pu, Y. P. Huang, Y. M. Liu, Q. J. Guan, and H. B. Ling. Edter: Edge detection with transformer. In *Proceedings of the IEEE/CVF conference on computer vision and pattern recognition*, pages 1402–1412, 2022.